Available online at www.sciencedirect.com
SCIENCE DIRECT®
Nuclear Instruments and Methods in Physics Research B 243 (2006) 272–276
NIM B
Beam Interactions with Materials & Atoms
www.elsevier.com/locate/nimb

Monte Carlo simulations of positrons transmission and backscattering probabilities in nickel

Asuman Aydın *

Balıkesir University, Faculty of Sciences and Literature, Department of Physics, 10100 Balıkesir, Turkey

Received 18 August 2005; received in revised form 22 September 2005
Available online 15 November 2005

Abstract

Monte Carlo simulations for positron backscattering from the semi-infinite nickel with normal angle of incidence and the transmission through nickel foils of isotropically implanted positrons from a ^{22}Na β^+ source is reported. The elastic scattering cross section, have been obtained from Rutherford differential cross section where the numerical coefficient in the atomic screening parameter and spin-relativistic correction factor is taken to be variable. Inelastic scattering model was employed to simulate the energy loss using Gryzinski's semi-empirical expression and Liljequist and Gryzinski models to calculate the total inelastic scattering cross section. The simulated results and the available experimental data are found to be in reasonable agreement.

PACS: 25.30.Hm; 24.10.Lx

Keywords: Monte Carlo simulations; Positron scattering; β^+; Transmission; Backscattering; Implantation; Nickel

1. Introduction

The electron and positron solid interaction is of great importance in the field of conventional transmission, scanning transmission, in the area of micro and optoelectronics. The study of electron and positron transmission and backscattering from metal films is important. Backscattering of electrons and positrons from thin films has impact on a range of surface science techniques [1–4].

Purely analytical models and simple approaches using closed formulas were not able to give satisfactory results. However, the rapid evolution of the computer calculation capability has made possible. A great deal of theoretical investigations and the Monte Carlo approach has been recognized as a powerful technique for performing certain calculations. The Monte Carlo simulation of positron transport is based on a stochastic description of the scattering process. The accuracy of the simulation depends entirely upon modeling the scattering processes. The dominant processes are elastic and inelastic scattering. The concept of scattering cross section is by itself defined as a statistical quantity being the probability that a positron is scattered. In other words, it is a target area that is statistically meaningful and which a positron would effectively see. When a positron beam impinges on a sample, some positrons, after doing a number of collisions with the atoms of target, reflected from the surface, while some other positrons penetrate a distance larger than the thickness of the material, and are thus transmitted and emerge from the back of the sample. The remaining positrons that have a penetration depth less than the thickness of the material and which are not backscattered are implanted in the target. The fractions of absorbed, backscattered and transmitted positrons depend on the thickness of the target.

Such a study ^{22}Na β^+ as positron emitter impinging on thin nickel target with normal angles of incidence has been

* Tel.: +90 266 2493358; fax: +90 266 2493360.
E-mail address: aydina@balikesir.edu.tr

0168-583X/$ - see front matter © 2005 Elsevier B.V. All rights reserved.
doi:10.1016/j.nimb.2005.10.002

made in the present paper using Monte Carlo simulation techniques.

2. Method

The simulation technique is mainly based on the screened Rutherford differential cross section [5] with a spin-relativistic correction factor for the elastic scattering at high energies supplemented by total cross sections at low energies. Gryzinski's the semi-empirical expression [6] is used to simulate the energy loss due to inelastic scattering, and Gryzinski [6] and Liljequist's model [7] to calculate the total inelastic scattering cross section. The detailed description of the Monte Carlo code and the calculation of cross sections have been reported elsewhere [8–10], only the differences are highlighted here.

2.1. Elastic scattering

The screened Rutherford cross section with the spin-relativistic factor [5] have been used for elastic scattering

$$\frac{d\sigma(\theta,E)}{d\Omega} = Z^2 r_e^2 \frac{1-\beta^2}{\beta^4} \frac{1}{(1-\cos\theta+2\eta)^2} K_{rel}(\theta,E), \quad (1)$$

where θ is the scattering angle, E is the kinetic energy of incoming positron, $Z = 28$, r_e is the classical electron radius, β is the speed of positron in units of c, η is the screening angle and $K_{rel}(\theta,E)$ is the spin-relativistic factor. $K_{rel}(\theta,E)$ is equal to the ratio of the Mott cross section to the Rutherford cross section, and its values for several energies and scattering angles have been tabulated by Doggett and Spencer [11], and Idoeta and Legarda [12]. An analytic expression for the spin-relativistic factor $K_{rel}(\theta,E)$ has been obtained as a function of

$$K_{rel}(\theta,E) = p_1(E) + p_2(E)\theta + p_3(E)\theta^2 + \cdots \quad (2)$$

the kinetic energy E of incident positrons and the scattering angle θ.

The angular dependence of the screened Rutherford cross section is given by the factor $1/(1-\cos\theta+2\eta)^2$. The screening angle η for positrons has been calculated by Nigam and Mathur [13] using the first and second Born approximations. By assuming a suitable value of η a reasonable angular distribution can be obtained, tried several energy dependent expressions for η but the expression

$$\eta = \exp(p_1 + p_2 x + p_3 x^2), \quad (3)$$

where, $x = \ln E$ (keV), $p_1 = -2.24902$, $p_2 = -0.91813$, $p_3 = -0.05743$, has given the optimum results. This expression has been obtained by taking $\eta = 0.98$ for $E = 50$ eV and some calculated values of η using the expression obtained with the first Born approximation for $E = 10$–600 keV and fitting a power expansion on $(\ln E, \ln\eta)$ points.

The calculation of elastic scattering cross section for $E < 25$ keV ($0.3Z^{4/3}$ keV) should be made with the partial wave expansion [5]. The total elastic cross section for positrons on nickel have been obtained by scaling the values for gallium atoms calculated by Öztürk et al. [14] in the energy region 50 eV to 2 keV. The total elastic cross sections have been calculated for several values of E in the range 25–600 keV by integrating the screened Rutherford cross section with the spin-relativistic factor. A continuous expression of the total elastic cross section needs as a function of E in the range 50 eV to 600 keV. Therefore, the expression has been obtained

$$\mu_e\ (cm^{-1}) = \exp(p_1 + p_2 x + p_3 x^2 + p_4 x^3), \quad (4)$$

$x = \ln E$ (keV), $p_1 = 15.92673$, $p_2 = -0.66347$, $p_3 = -0.093988$, $p_4 = 0.0175172$ by fitting a power expansion on $(\ln E, \ln\mu_e)$ points.

2.2. Inelastic scattering

The total inelastic scattering cross section can be calculated using the models given by Liljequist [7]. The following expression is used to fit the values calculated from Liljequist's model for the macroscopic total inelastic cross section:

$$\mu_i\ (cm^{-1}) = \exp(p_1 + p_2 x + p_3 x^2 + p_4 x^3), \quad (5)$$

where $x = \ln E$ (keV), $p_1 = 15.893$, $p_2 = -0.75523$, $p_3 = -0.0605584$, $p_4 = 0.0116912$ by doing a fit over $(\ln E, \ln\mu_i)$ points. The total ionization cross section, calculated from Gryzinski's excitation function [6], has been used to determine the electron shell from which the scattering occurred. Then, the energy loss in the inelastic scattering process using Gryzinski's excitation function [6] has been sampled.

Treatment of the elastic and inelastic collisions, which has been explained above, contains several approximations. As a result the total cross sections given by Eqs. (4) and (5) could have uncertainties which are estimated to be of the order of 10–20%. These uncertainties give us the freedom to optimize the total cross section values to obtain results which are as close as possible to the experimental values. The calculation results, which are presented below have been obtained by using the μ_e and μ_i in Eqs. (4) and (5) multiplied by an overall factors.

A schematic diagram of the model is depicted in Fig. 1. Elastic and inelastic scattering are assumed to produce

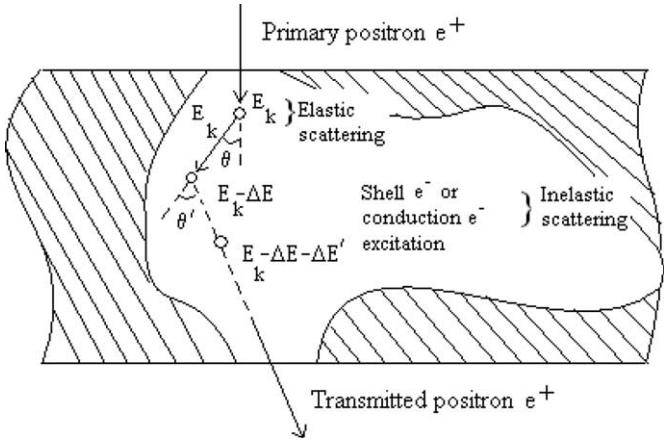

Fig. 1. Scheme of elastic and inelastic scattering in a film target.

angular direction. The computer codes have been written for foils of various thicknesses and semi-infinite geometries and for ^{22}Na β^+ source and monoenergetic positron beams. The positrons in a semi-infinite medium or foils of various thicknesses have been followed until they have backscattered or transmitted or slowed down below 50 eV. A typical run involves the computation of 10 000 trajectories. The time required to compute a single trajectory clearly depends on the initial energy and on the material.

3. Results and conclusions

3.1. Slab geometry

The measurements of transmission of positrons emitted from a ^{22}Na β^+ source as a function of Ni foil thickness were done by Hansen et al. [15] and Linderoth et al. [16]. In addition, the penetration of positrons from a ^{22}Na β^+ source into Ni foils sandwiched between different backscattering materials (Ni, Mo, NaCl, Kapton) has been studied for the geometry commonly used in PAT experiments by Hansen et al. [15] and Linderoth et al. [16].

The energy of positrons emitted from a ^{22}Na β^+ source was sampled using the theoretical spectrum Konopinski [17] assuming that positrons emitted isotropically from the source and the transmission probabilities were determined for the various thicknesses of nickel.

According to the best of my knowledge no additional experimental results and/or any theoretical calculations for the transmission and backscattering probabilities of positrons and β^+ for nickel have been reported in the last decade. In this study, the transmitted and reflected fractions of positrons emitted from ^{22}Na β^+ source as a function of thickness have been simulated.

Mahony et al. [18] have given an expression for the transmission of positrons through a foil thickness, x. α is the absorption coefficients of the foil and β is the backscattering coefficient of the backing material.

$$T(x) = \frac{(1-\beta)\exp(-\alpha x)}{1-\beta\exp(-2\alpha x)}. \tag{6}$$

α, is derived specifically from the empirical relation for ^{22}Na

$$\alpha = \frac{2.8\rho Z^{0.15}}{\overline{E}^{1.19}}\ (\mathrm{cm}^{-1}), \tag{6a}$$

where, ρ is the density in g/cm^3, Z is the atomic number and $\overline{E}$ is the mean energy for the ^{22}Na β^+ distribution, equal to 0.15 MeV. β, is a function of the atomic number, Z and is empirically described by

$$\beta = 0.342\log Z - 0.416. \tag{6b}$$

Monte Carlo calculations for the transmission rate of using a ^{22}Na β^+ source in the range 1–75 mg/cm^2 thicknesses nickel have been performed for a comparison with the experimental results. The calculated transmission probabilities in nickel are well agreed with the expression of Mahony et al. [18] and the experiment of Hansen et al. [15]. The results obtained from the analog Monte Carlo code and calculated using (6) are plotted in Fig. 2 for nickel. Relative proportions at ($E_{max} = 0.542$ MeV) ^{22}Na β^+ transmitted and reflected for the various thicknesses Ni target are shown in Fig. 3. The energy distributions of the transmitted β^+ for the various thicknesses of nickel have been calculated. Fig. 4 shows the energy distribution of the transmitted and reflected β^+, for 28 mg/cm^2 thickness. The angular

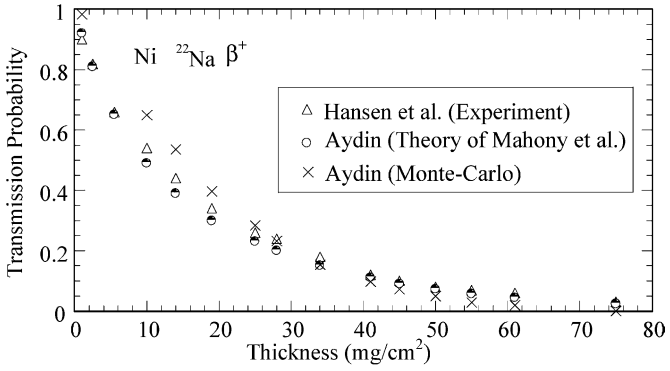

Fig. 2. Transmission probabilities as a function of β^+ energy for Ni in comparison with the experimental data of Hansen et al. [15] and calculated from expression of Mahony et al. [18].

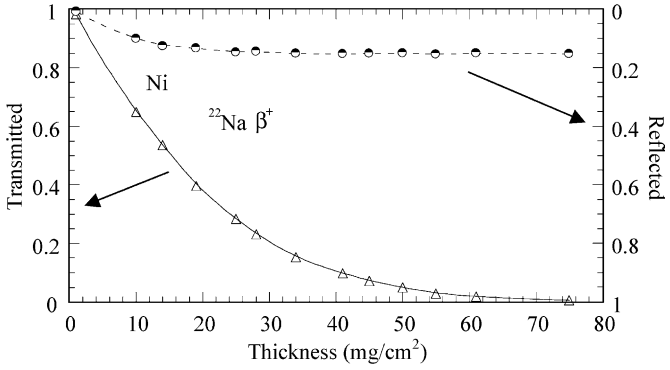

Fig. 3. Relative proportions β^+ transmitted (full curve) and reflected (dashed curve) as a function of thicknesses for Ni target.

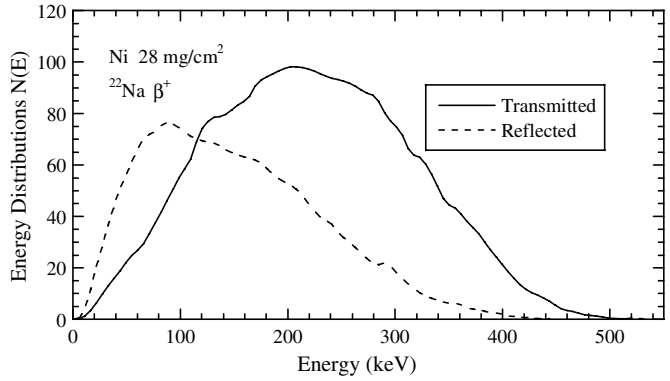

Fig. 4. Theoretical energy distributions of transmitted and reflected β^+ for Ni target at 28 mg/cm^2 thickness.

distribution of transmitted β^+ has also been calculated from the present Monte Carlo calculation for nickel as well as the energy distribution. The result is shown in Fig. 5.

3.2. Semi-infinite geometry

The energy and angular distributions, backscattering probabilities and mean penetration depths of positrons entering into the semi-infinite nickel target were also studied. Fig. 6 presents the calculated mean penetration depth $\langle z \rangle$ of positrons as a function of their energy at normal incident angle. Fig. 7 shows the calculated backscattering probabilities for positrons entering normally into the semi-infinite nickel as a function of energy. Direct measurements of doubly differential (angle and energy) distributions of backscattered positrons are reported by Massoumi et al. [19] for only 35 keV positrons incident normally on the target ($4 \leqslant Z \leqslant 82$). In Fig. 7, the calculated backscattering probability was found to be 0.163, while the measurements of Massoumi et al. [19] was 0.164, for 35 keV the energy. Fig. 8 shows the energy distributions of backscattered positron in the semi-infinite nickel normally incident angle for 35 keV the positron energy. The angular distribution of backscattered positrons has also been calculated from the present Monte Carlo calculation for semi-infinite nickel as well as the energy distribution. Fig. 9 indicates the positrons angular distribution for 0° incident angle at 35 keV. Typical implantation profiles for positrons at the same angle and energy are shown in Fig. 10. The reflection probability of positrons was calculated from a ^{22}Na β^+ source located at the boundary of a semi-infinite nickel target to be 0.412.

A Monte Carlo simulation based on screened Rutherford differential scattering cross section and approximate energy loss expression has been used to transmission and backscattering probabilities of β^+ and positrons normally

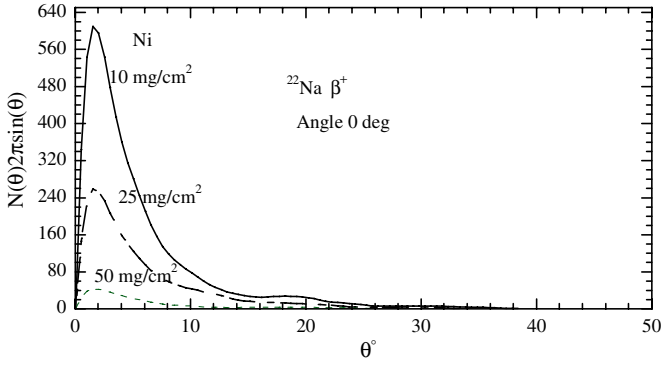

Fig. 5. Theoretical angular distributions of transmitted β^+ in Ni target at 10, 25 and 50 mg/cm^2 thicknesses.

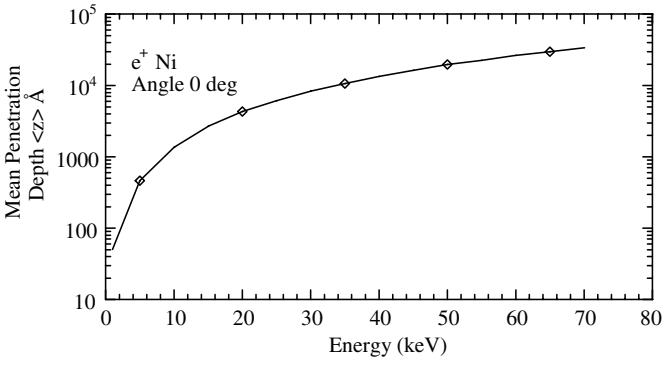

Fig. 6. Mean penetration depth $\langle z \rangle$ as a function of positron energy.

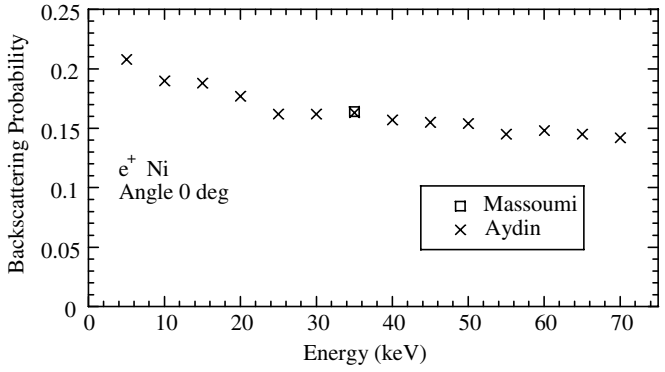

Fig. 7. Comparison of backscattering probabilities for Ni.

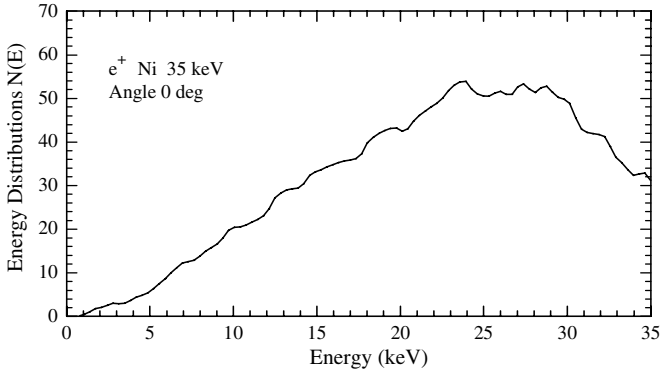

Fig. 8. Energy distributions of backscattered positrons from the semi-infinite nickel target at 35 keV positron energy and the incident angles of zero degree.

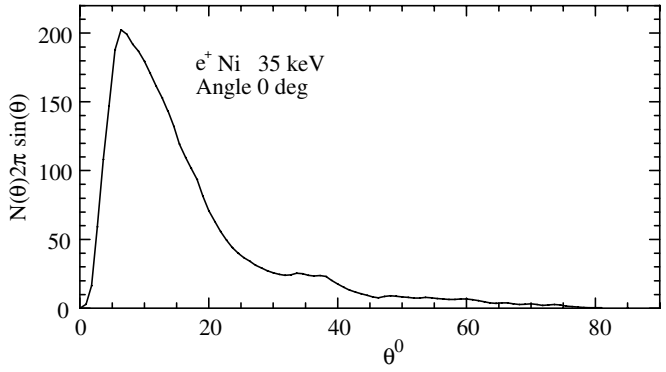

Fig. 9. Theoretical angular distributions of transmitted positrons at 35 keV energy for semi-infinite Ni.

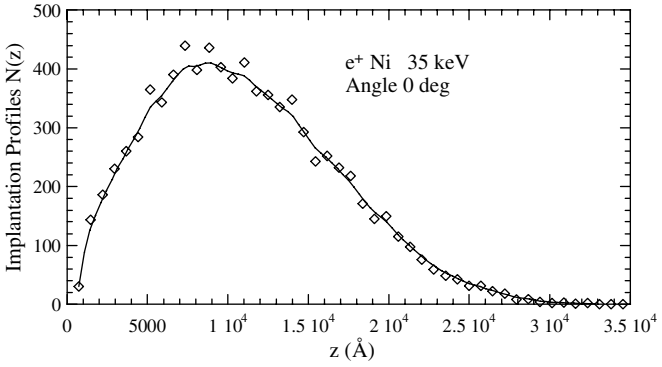

Fig. 10. Typical implantation profiles of positrons at 35 keV, zero degree incident angles in the semi-infinite Ni.

incident nickel. The energy and angular distributions and the positron implantation profile have also been investigated. Good agreement is found with the existing experimental data in the literature. Although the basic physical mechanisms of positron solid interactions are reasonably well understood, the intensive research during the last years has produced many exciting developments.

References

[1] A.P. Mills Jr., P.M. Platzman, B.L. Brown, Phys. Rev. Lett. 41 (1978) 1076.
[2] A.P. Mills Jr., Phys. Rev. Lett. 41 (1978) 1828.
[3] A.P. Mills Jr., L. Pfeiffer, Phys. Rev. Lett. 43 (1979) 1961.
[4] H. Niedrig, J. Appl. Phys. 53 (1982) R15, and references cited therein.
[5] S.M. Seltzer, Appl. Radiat. Isot. 42 (1991) 917.
[6] M. Gryzinski, Phys. Rev. A 138 (1965) 305, 322, 336.
[7] D. Liljequist, J. Phys. D: Appl. Phys. 16 (1983) 1567.
[8] E.N. Ozmutlu, A. Aydın, Appl. Radiat. Isot. 45 (9) (1994) 963.
[9] A. Aydın, Nukleonika 46 (3) (2001) 87.
[10] A. Aydın, Nukleonika 50 (1) (2005) 37.
[11] J.A. Doggett, L.V. Spencer, Phys. Rev. 103 (6) (1956) 1597.
[12] R. Idoeta, F. Legarda, Nucl. Instr. and Meth. B 71 (1992) 116.
[13] B.P. Nigam, V.S. Mathur, Phys. Rev. 121 (1961) 1577.
[14] N. Öztürk, W. Williamson Jr., A.J.J. Antolak, Appl. Phys. 70 (2) (1991) 537.
[15] H.E. Hansen, S. Linderoth, K. Petersen, Appl. Phys. A 29 (1982) 99.
[16] S. Linderoth, H.E. Hansen, B. Nielsen, K. Petersen, Appl. Phys. A 33 (1984) 25.
[17] E.J. Konopinski, The Theory of Beta Radioactivity, Oxford University Press, London, 1966, 7.
[18] J. Mahony, T. Friessnegg, G. Tessaro, P. Mascher, W. Puff, Appl. Phys. A 63 (1996) 299.
[19] G.R. Massoumi, N. Hozhabri, W.N. Lennard, P.J. Schultz, Phys. Rev. B 44 (7) (1991) 3486.